Available online at www.sciencedirect.com
SCIENCE DIRECT®
International Journal of Heat and Fluid Flow 24 (2003) 736–746
International Journal of HEAT AND FLUID FLOW
www.elsevier.com/locate/ijhff

Combined gas radiation and laminar mixed convection in vertical circular tubes

EzEddine Sediki [a], Anouar Soufiani [b,*], Mohamed Salah Sifaoui [a]

[a] *Laboratoire de Rayonnement Thermique, Faculté des Sciences de Tunis, 2092 El Manar, Tunis, Tunisie*
[b] *Laboratoire d'Énergétique Moléculaire et Macroscopique, Combustion (EM2C), UPR 288 du CNRS, École Centrale Paris, 92295 Châtenay-Malabry Cedex, France*

Received 26 October 2002; accepted 8 February 2003

Abstract

A numerical study of the interaction between thermal radiation and laminar mixed convection for ascending flows of emitting and absorbing gases in vertical tubes is presented. The radiative properties of the flowing gases, H_2O, CO_2 and H_2O–CO_2 mixtures are modeled by using the global absorption distribution function model. The temperature-dependent thermophysical properties are considered when solving the flow field and energy balance equations. Results are presented in terms of velocity and temperature fields, and of evolution of centerline velocity, friction factor and heat fluxes. The effects of radiation on the regime of reverse flow occurrence are also examined. It is shown that, for heated gases, radiation tends to reduce the velocity distortion effect of buoyancy. Radiative transfer delays then significantly the occurrence of reverse flow for heated gases while, for cooled gases, the flow regime is practically not affected.

Keywords: Gas radiation; Mixed convection; Coupled heat transfer; Vertical ducts

1. Introduction

Thermal radiation with simultaneous buoyancy and forced convection is an important issue for applications such as heat exchangers and cooling processes in nuclear reactors. In such systems, heat transfer results from coupled processes, in general, cannot be calculated separately. When the flowing medium is a radiating molecular gas, its complex absorption and emission spectra introduce an important difficulty in the simulation of these flows. Viskanta (1998), in a literature overview on coupled heat transfer in high temperature gas flows, pointed out the modeling difficulties and the resulting non-complete understanding of these coupled processes. In general, the computational methods for solving the radiative transfer problem with its spectral nature, based on directional, spatial and rigorous spectral discretizations still remain prohibitive in terms of computing time and storage capacity. In view of this fact, most of the studies available in the literature on combined thermal radiation and mixed convection are based on simplifying assumptions such as gray gases.

For non-radiating fluids in vertical channels and tubes, in both cases of buoyancy-assisted flow (heated ascending or cooled descending flows) or opposed flow (heated descending or cooled ascending flows), much work, both theoretical and experimental, has been conducted in mixed convection flows and reviewed by Jackson et al. (1989), Jeng et al. (1992), Gau et al. (1992a,b), Wang et al. (1994) and Jones and Ingham (1994) among others. In general, these investigations concerned the distortion effect that buoyancy forces have on the axial velocity and temperature distribution inside the channel or the transition to turbulent flow at some point along the duct. In the formulation of the convective heat transfer problem, two approaches are pointed out depending on the inclusion or the exclusion of the axial diffusion term in the governing momentum and energy equations. Namely, the available investigations have been performed either (i) by using parabolic methods which neglect the axial diffusion (Aung and Worku, 1986a,b; Aung et al., 1991; Habchi and Achaya,

* Corresponding author. Tel.: +33-141-13-1031; fax: +33-147-02-8035.
E-mail address: soufiani@em2c.ecp.fr (A. Soufiani).

0142-727X/$ - see front matter © 2003 Elsevier Inc. All rights reserved.
doi:10.1016/S0142-727X(03)00005-5

Nomenclature

a_j	quadrature weights
C_p	specific heat at constant pressure [J kg^{-1} K^{-1}]
D	diameter of the duct [m]
g	gravity acceleration [m s^{-2}]
Gr	Grashof number $= g\beta(T_w - T_0)\rho^2 R^3/\mu^2$
h	enthalpy per unit mass [J kg^{-1}]
I	radiative intensity [W m^{-2} s t^{-1}]
k	reduced absorption coefficient [m^{-1} Pa^{-1}]
L_0	upstream region length [m]
L	downstream region length [m]
Nu	Nusselt number
p	pressure [Pa]
Pr	Prandtl number $= \mu C_p/\lambda$
Pe	Peclet number $= RePr$
q	heat flux per unit area [W m^{-2}]
r	radial coordinate [m]
R	radius of the duct [m]
Re	Reynolds number $= u_m D\rho/\mu$
Rp	integrated radiative power per unit volume [W m^{-1}]
s	curvilinear abscissa [m]
S	cross sectional area [m^2]
T	temperature [K]
T_b	bulk temperature [K]
u	axial velocity [m s^{-1}]
u_c	axial centerline velocity [m s^{-1}]
u_m	mean axial velocity [m s^{-1}]
v	transverse velocity [m s^{-1}]
x	flow direction [m]
X_l	molar fraction of the absorbing species l

Greeks

β	thermal expansion coefficient [K^{-1}]
ϵ	emissivity
κ	absorption coefficient [m^{-1}]
λ	molecular thermal conductivity [W m^{-1} K^{-1}]
μ	viscosity [kg m^{-1} s^{-1}]
ν	wave number [m^{-1}]
ρ	density [kg m^{-3}]
τ	dimensionless wall shear stress $= -\mu(\partial u/\partial r)_{r=R}/(\rho u_m^2/2)$
σ	Stefan–Boltzmann constant [W m^{-2} K^{-4}]
Ω	solid angle

Subscripts

cd	conductive
i	discretization over x-direction
j	discretization of absorption coefficients
o	inlet conditions
ref	reference
r	radiative
tt	total
w	wall
ν	monochromatic quantity

Superscript

°	equilibrium radiation

1986; Ingham et al., 1988; Jones and Ingham, 1994) or (ii) by solving the full elliptic equations (Zeldin and Schmidt, 1972; Morton et al., 1989; Ingham et al., 1990; Heggs et al., 1990; Nesreddine et al., 1998).

These studies demonstrate that when the magnitude of both Reynolds and Peclet numbers are sufficiently large, the boundary-layer approximation leads to accurate results. The parabolic boundary-layer equations are solved by using a marching technique up to a point where either the flow becomes fully developed or flow reversal is detected near the center of the duct or close to the wall. When flow reversal occurs, the marching solution procedure may diverge at, or near, the point of separation because the direction of the flow and of the marching technique oppose each other. Ingham et al. (1988) overcame the numerical instability of these flow reversals by using an iterative method.

The major advantage of parabolizing the equations is the opportunity to use a marching technique which saves computing time and storage capacity. This assumption, when applicable, offers a reasonable compromise for treating the non-gray two-dimensional radiative problem with an acceptable accuracy by using the numerical procedure presented by Sediki et al. (2002) which transforms the elliptic radiative transfer problem to a series of parabolic problems.

Concerning radiatively participating fluids in vertical channels, thermal radiation effects on laminar mixed convection have not been extensively studied. Besides neglecting the axial radiation component, the studies conducted by Yang (1991, 1992) for flows in vertical circular ducts and by Yan and Li (1997, 2001) for flows in inclined or vertical square ducts were applied to gray media. The authors concluded that heat transfer is enhanced by the presence of radiation, but the thermal buoyancy effect is reduced. Despite the numerous studies related to non-radiating or gray fluids, the effects of real gas radiation on mixed convection and on the reverse flow occurrence regime have not been explored. This motivates our investigation.

In the present paper, numerical calculations are performed to study the effects of gas radiation, with its spectral nature, on simultaneously developing hydrodynamic and thermal fields for a steady laminar as-

cending flow in a heated or cooled vertical circular duct. The flow and energy balance equations are solved simultaneously by using an implicit finite-difference technique with temperature-dependent fluid properties. To solve the radiative part of the problem, a numerical procedure, detailed by Sediki et al. (2002), is simultaneously used with the parabolic boundary-layer equations of the flow. The radiative properties of the flowing gases are modeled by using the absorption distribution function (ADF) model (Pierrot et al., 1999a,b). A discrete-direction method is applied to solve the geometrical part of radiative transfer (Zhang et al., 1988; Sediki et al., 2002). In Section 2, we recall briefly the basic equations, the radiative property model and the numerical methods used to solve them. In Section 3, we first present radiation effects on mixed convection of H_2O, CO_2 and H_2O–CO_2 laminar flows. Effects on temperature and velocity profiles, as well as on heat fluxes and friction factors are presented. Then, we discuss the effect of thermal radiation on the regime of reverse flow occurrence.

2. Basic formulation and methods of solution

2.1. Basic equations

We consider an ascending developing steady laminar axisymmetric flow of a non-scattering H_2O, CO_2, or H_2O–CO_2 mixture in a heated or cooled vertical circular duct at atmospheric pressure (see Fig. 1). This is for instance the case of regenerative exchangers used for energy recuperation from combustion products, or a vertical linear concentrated solar collector where infrared active gases could be used to enhance heat transfer, or the case of water vapor flows in some nuclear heat exchangers. The above applications are in general in an intermediate regime between constant wall temperature and constant wall flux. We assume here a constant wall temperature to gain insight on the effects of radiative transfer on global heat transfer. Two cases will be examined. The first is the buoyancy-assisted flow which corresponds to the heated ascending flow (positive Gr). The second is the buoyancy-opposed flow which corresponds to the cooled ascending flow (negative Gr). We assume that the gas flow rate is fixed by some metering device.

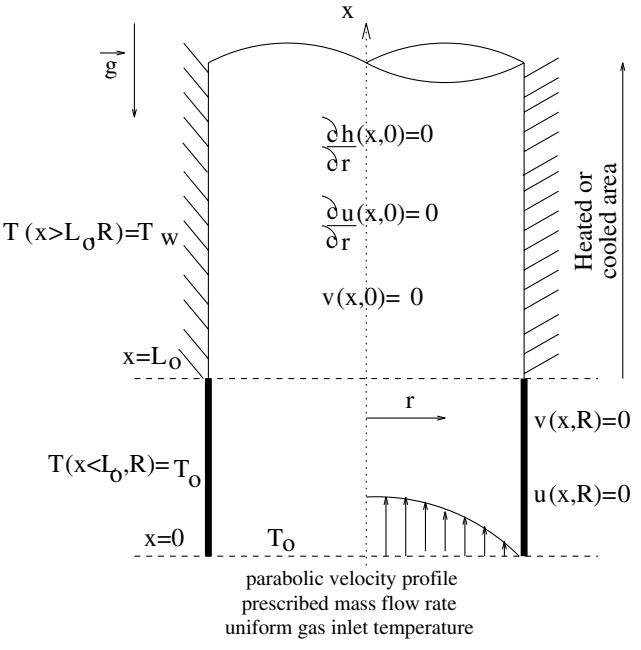

Fig. 1. Geometry and boundary conditions.

In the formulation of heat transfer and fluid flow without radiation, the usual boundary-layer approximations are made. If we restrict our considerations to steady, axially symmetric flows with the x-axis vertically upwards, the mass, momentum and energy balance equations, written in cylindrical coordinates, are given by:

$$\frac{\partial(\rho r u)}{\partial x}+\frac{\partial(\rho r v)}{\partial r}=0, \tag{1}$$

$$\frac{\partial(\rho u u)}{\partial x}+\frac{\partial(\rho u v)}{\partial r}=-\frac{\mathrm{d}p}{\mathrm{d}x}-\rho g+\frac{1}{r}\frac{\partial}{\partial r}\left(r\mu\frac{\partial u}{\partial r}\right), \tag{2}$$

$$\frac{\partial(\rho u h)}{\partial x}+\frac{\partial(\rho v h)}{\partial r}=-u\frac{\mathrm{d}p}{\mathrm{d}x}+\frac{1}{r}\frac{\partial}{\partial r}\left(r\frac{\lambda}{C_p}\frac{\partial h}{\partial r}\right)+\mu\left(\frac{\partial u}{\partial r}\right)^2-\nabla\cdot\mathbf{q}_{\mathrm{r}}, \tag{3}$$

where u and v are the axial and radial velocity components, respectively, h, ρ, μ, λ and C_p designate the enthalpy per unit mass, the temperature-dependent density, viscosity, thermal conductivity and specific heat at constant pressure, respectively, and $\mathbf{q}_{\mathrm{r}}$ is the radiative vector flux.

The boundary conditions for the considered problem are summarized in Fig. 1. At the wall the no-slip condition, the impermeability of the wall, and the imposed wall temperature give the following boundary conditions:

$$u(x,R)=0,\quad v(x,R)=0, \tag{4}$$

$$h(x,R)=h(T_{\mathrm{w}})\quad \text{for } x>L_0 \quad \text{and}$$
$$h(x,R)=h(T_0)\quad \text{for } x<L_0.$$

The isothermal length allows to account for realistic radiative inlet conditions with the possibility of preheating or precooling of the gas before the section $x=L_0$.

At the centerline the following conditions arise from the symmetry of the problem:

$$\left.\frac{\partial u(x,r)}{\partial r}\right|_{r=0} = 0, \quad v(x,0) = 0 \quad \text{and} \quad \left.\frac{\partial h(x,r)}{\partial r}\right|_{r=0} = 0. \tag{5}$$

For $x = 0$ we have the inlet conditions:

$$v(0,r) = 0, \quad u(0,r) = 2u_0\left(1 - \left(\frac{r}{R}\right)^2\right) \quad \text{and} \quad h(0,r) = h(T_0), \tag{6}$$

where u_0 (or the flow rate) is assumed to be fixed by a metering device. No flow boundary conditions are required at the outlet section of the computational domain since the problem under consideration is assumed parabolic in x direction.

The significant temperature difference imposed between the walls and the gas requires the use of temperature-dependent fluid properties.

The gas mixtures are assumed to obey the perfect gas law and the thermophysical properties are approximated by temperature-dependent functions generated from the data given in Touloukian et al. (1970a,b) for pure gases. For mixtures, we used the Buddenberg–Wilke approximation for μ and the Mason–Saxena approximation for λ (see Touloukian et al., 1970a,b).

2.2. Gas radiation modeling

Gas radiative properties are represented by the ADF model (Pierrot et al., 1999a). This global model is limited to gray walls and is sufficiently accurate for moderate temperature gradients. Comparisons between the results from the ADF model and from the more elaborated correlated-k band model, applied to the study of combined forced convection and radiation, have shown a reasonable accuracy of the ADF model (Sediki et al., 2002). For each absorbing species, the ADF model parameters are the reduced absorption coefficients (k_j, $j = 1, \ldots, N$) corresponding to values of $\kappa_v/(pX_l)$ (l being H_2O or CO_2), and the corresponding weights a_j satisfying $\sum_j a_j = 1$. The parameters used for pure H_2O or pure CO_2 are those developed by Pierrot et al. (1999b).

For H_2O, the parameters were tabulated for five X_{H_2O} values but they do not significantly depend on X_{CO_2} when CO_2 is the absorbing gas. The chosen reference conditions were $T_{ref} = 1100$ K and $X_{H_2O,ref}$ or $X_{CO_2,ref}$ equal to 0.1 since the model was first devoted to general combustion applications. These parameters have been calculated at atmospheric pressure and different temperatures from the spectroscopic EM2C data bases (Rivière et al., 1995; Scutaru et al., 1994), with $N = 8$ (one gas corresponding to the transparency regions and seven active gases).

Different implementations of the ADF model have been discussed by Taine and Soufiani (1999) for mixtures of absorbing gases. For H_2O–CO_2 mixtures considered here, the molar fractions imposed are $X_{H_2O} = 0.45$ and $X_{CO_2} = 0.55$, which roughly corresponds to the combustion of heavy fuels with pure oxygen. The mixture is treated as a single gas with the spectral absorption coefficient $\kappa_v = \kappa_{v,H_2O} + \kappa_{v,CO_2}$. Specific parameters for this mixture, at atmospheric pressure, were developed for the purpose of the present study. The same spectroscopic data bases, reference temperature, and number of gray gases were considered as for single absorbing species.

The total radiative intensity $I(\mathbf{u}, s)$ at s and for the direction $\mathbf{u}$ is written as the sum of the partial intensities:

$$I(\mathbf{u}, s) = \sum_{j=1}^{N} I_j(\mathbf{u}, s). \tag{7}$$

Each partial intensity $I_j(\mathbf{u}, s)$ satisfies the radiative transfer equation:

$$\frac{\partial I_j(\mathbf{u}, s)}{\partial s} = k_j(s) X_l p(s) \left[a_j(s)\frac{\sigma T^4(s)}{\pi} - I_j(\mathbf{u}, s)\right]. \tag{8}$$

The divergence of the radiative flux, appearing in the energy equation, is given by:

$$\nabla \cdot \mathbf{q}_r(s) = \sum_{j=1}^{N=8} k_j(s) X_l p(s) \int_{4\pi} \left[a_j(s)\frac{\sigma T^4(s)}{\pi} - I_j(\mathbf{u}, s)\right] \mathrm{d}\Omega. \tag{9}$$

For the radiative boundary conditions, the walls are assumed to emit and reflect isotropically with constant wall emissivity ϵ_w. Although calculations have been carried out with various emissivities, we limit ourselves to black walls in this presentation. In addition, the inlet section ($x = 0$) is considered for radiative transfer as a black wall at temperature T_0 while the outlet section ($x = L_0 + L$) is considered as a perfectly reflecting wall at T_w. L is chosen sufficiently large so that this last condition has no incidence on the results near $x = L_0$. For each value of j, the geometrical part of the radiative transfer equation is solved by using a discrete-direction method described in Zhang et al. (1988) and Sediki et al. (2002).

2.3. Methods of solution

Radiative transfer calculations have been carried out both with the approximation of a locally one-dimensional temperature field and with the full two-dimensional temperature field. In the first case, the problem is parabolic and a marching procedure is applied. In the second case, we use an iterative procedure to reduce the elliptic problem to a series of parabolic ones. This procedure is similar to the one developed in Sediki et al.

(2002) for coupled forced convection and radiation in circular ducts. Flow and temperature calculations, up to the outlet section, are first carried out with the radiative flux divergence obtained from the 1D approximation. The resulting 2D temperature field is then used to compute a new radiative field, which enables new parabolic calculations of the flow and temperature fields, and so on, until the convergence of the coupled fields. In general, only three or four iterations are required for convergence. For each parabolic calculation, the velocity and temperature fields are computed by using a marching implicit finite volume procedure based on the pressure correction algorithm up to a point where either the flow becomes fully developed or reverse flow is detected near the center of the duct or adjacent to the cold wall. A constant mesh size is used for the radial direction and a variable one in the axial direction. This mesh size increases far from the entrance, which provides a higher accuracy in the regions of pronounced temperature and velocity gradients. Typically, we use 80 radial points and 20,000 axial ones to compute the flow field. But such a refined grid is not required for 2D radiation calculations; numerical tests showed that typically 20×100 nodes are sufficient. Numerical interpolations and extrapolations are used to convert the results from the convective grid mesh to the radiative one and vice versa.

Table 1 shows that doubling the convective grid introduces less than 0.3% differences for both conductive and radiative fluxes. In the same manner, doubling the radiative grid yields less than 1.5% difference for radiative fluxes in the configuration considered in Section 3.

The convection part of this procedure was first validated by comparison with the results of Backstron and McEligot (1970) for laminar forced convection and temperature-dependent fluid properties. It was then applied to laminar mixed convection and compared to the results of previous studies where the boundary-layer assumption was used (Marner and McMillan, 1970; Worsoe-Schmidt and Leppert, 1965). The relative difference, in terms of Nusselt number, between our results and those from previous investigations do not exceed 2%.

However, neglecting the contributions of axial diffusion of momentum and energy in the system of equations is a crucial approximation for the kind of flows considered in this study. Worsoe-Schmidt and Leppert (1965) concluded that, for developing flows in circular ducts, the boundary-layer model is valid for $x/(R \cdot Re \cdot Pr)$ greater than typically 10^{-3}. The range of validity of this assumption has been also extensively discussed by El-Shaarawi and Sarhan (1981), Aung and Worku (1986a) and Jeng et al. (1992) among others.

In this study, we have on one hand checked that for all the studied configurations presented in Section 3.1, the neglected axial terms (computed from the numerical solutions) are negligible in comparison with the corresponding radial ones. On the other hand, we made specific computer runs to compare our parabolic results with the available previous calculations using the full elliptic equations, but with the Boussinesq approximation.

Specific calculations have been carried out to reproduce the local friction factor τRe in the same considerations as Wang et al. (1994), i.e., $Pr = 0.71$, $Pe = 71$ and $|Gr/Re| = 10$. The dimensionless wall shear stress τ is defined as $-\mu(\partial u/\partial r)_{r=R}/(\rho u_m^2/2)$. The local Nusselt number obtained in the same conditions have been also compared with the results of Wang et al. (1994) and with the results of Zeldin and Schmidt (1972), corresponding to a heated fluid with $Re = 500$, $Pe = 252.5$ and $|Gr/Re| = 30$ (mixed convection) or $|Gr/Re| = 0$ (forced convection) have also been done. The comparisons show that, for both friction coefficient and Nusselt number, the difference between parabolic and elliptic calculations do not exceed 5% for $x/(R \cdot Pe) \geqslant 5.0 \times 10^{-3}$ and that the differences decrease downstream. These comparisons indicate that the parabolic model is a reasonable approach for the prediction of heat transfer and fluid flow when no flow reversal occurs along the flow.

3. Results and discussion

The considered gases are pure H_2O, pure CO_2 or H_2O–CO_2 mixtures at atmospheric pressure with uniform molar fraction throughout the medium. The velocity inlet profile is assumed parabolic and the gas inlet temperature is constant. The calculations have been

Table 1
Conductive (q_{cd}) and radiative (R_p) fluxes obtained with three different convective grids

x (m)	$40 \times 10{,}000$		$80 \times 20{,}000$		$160 \times 40{,}000$	
	$\lvert q_{cd}\rvert$	$\lvert R_p\rvert$	$\lvert q_{cd}\rvert$	$\lvert R_p\rvert$	$\lvert q_{cd}\rvert$	$\lvert R_p\rvert$
0.5	395.44	508.20	399.76	510.48	398.70	509.40
1.0	193.62	329.73	195.18	346.08	194.83	345.44
1.50	118.06	237.51	119.04	238.92	118.87	238.50
2.0	74.50	159.48	75.17	160.65	75.11	160.45
2.50	47.42	105.13	47.90	106.05	47.89	105.99
3.0	30.33	68.80	30.68	69.51	30.69	69.52

Heated pure H_2O flow, $T_0 = 400$ K, $T_w = 800$ K and $Re = 2390$ (q_{cd} and R_p are defined in Section 3.1).

carried out either by including 2D radiative transfer or for the same flow with the medium considered as transparent. The Reynolds numbers were chosen sufficiently large ($\geqslant 200$) in order to neglect the effects of axial diffusion.

The presentation and discussion of the results will be divided into two subsections. The effects of radiative transfer on temperature and velocity fields, on friction coefficient and on heat fluxes are presented in Section 3.1. We compare in this section the results obtained with and without radiative transfer, but with the same prescribed flow rate and with the same inlet and wall temperatures. The influence of thermal radiation on the regime of the reverse flow occurrence is discussed in Section 3.2. In the following, the values of non-dimensional numbers (Re, Pr, Gr, Pe) are specified with gas thermophysical properties calculated at the inlet temperature T_0.

3.1. Radiation effects on the development of velocity and temperature fields

The flow and heat transfer mechanisms are governed by a great number of parameters resulting from the temperature-dependent fluid properties and its complex absorption spectra. Consequently, the results cannot be gathered in non-dimensional form. Although, several computations have been conducted for various gases and various combinations of these parameters, we limit ourselves, in this presentation, to some examples to illustrate the interaction between thermal radiation and mixed convection.

We consider a radiating gas flowing upward a vertical tube of diameter $D = 0.06$ m, if not specified elsewhere. The inlet and wall temperatures are $T_0 = 400$ K and $T_w = 800$ K, respectively, if the gas is heated, and $T_0 = 800$ K and $T_w = 400$ K in the cooling case. The inlet region has a length $L_0 = 0.3$ m. For comparison purposes, calculations have been done for the same gas considered as transparent with the presence of buoyancy forces (mixed convection) and without buoyancy forces (forced convection).

For heating H_2O (aiding buoyancy), typical results for the axial velocity and temperature profiles at different locations are presented in Fig. 2. Without radiation and buoyancy effects, the parabolic velocity shape is maintained downstream the section $x = L_0$ and the flow is simply accelerated due to the decrease of the density. When buoyancy effect is taken into account, the initial parabolic velocity profile is gradually distorted. Since the temperature increases near the wall, fluid density decreases and the flow is accelerated in this region. But as the flow rate in the duct is constant, the centerline velocity must correspondingly decrease. After a minimum is reached, the centerline velocity starts increasing and tends again to a parabolic profile corresponding to a

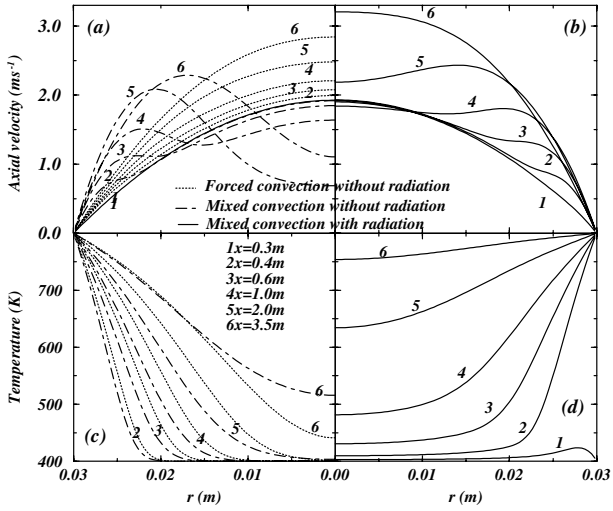

Fig. 2. Evolution of axial velocity and temperature profiles for heated H_2O, $Re = 2390$ and $|Gr/Re| = 190$. Forced and mixed convection without radiation (a) and (c). Coupled mixed convection, radiation (b) and (d).

fully developed isothermal flow. The evolution of the axial velocity profiles when accounting for radiative transfer are represented in Fig. 2b. When the flow goes downstream, the effect of radiation becomes significant and tends simultaneously to reduce the velocity near the wall and to increase it in the center of the duct. In fact, radiative transfer from the wall acts at distance and leads to a more pronounced heating in the central region of the duct. The flow is then accelerated in this region and slightly decelerated near the wall. This behavior shows that radiation tends to reduce buoyancy effects as pointed out by Yang (1991, 1992) and Yan and Li (1997, 2001) for gray media. Fig. 2c and d illustrate the evolution of the temperature profiles without and with radiation, respectively. The evolution of the temperature profile towards the wall temperature is obviously faster with radiation than without radiation. Even for diameters as small as 0.06 m, radiative transfer is shown to be more efficient than convective transfer in the conditions of Fig. 2. The comparison of the temperature profiles with and without radiation shows the presence of a preheating zone near the entrance ($x = L_0$) due to the propagation of radiation into the upstream region. The axial radiative flux component has a noticeable but small effect leading to an increase of gas temperature before $x = L_0$.

Fig. 3 shows the evolution of the local friction factor computed for coupled mixed convection and radiation and for mixed convection alone with $D = 0.03$ and 0.06 m. As the flow goes downstream, radiation tends to reduce the velocity near the wall and the local friction factor is strongly decreased. The product τRe tends to the constant value corresponding to the fully developed flow much more quickly when radiation is taken into

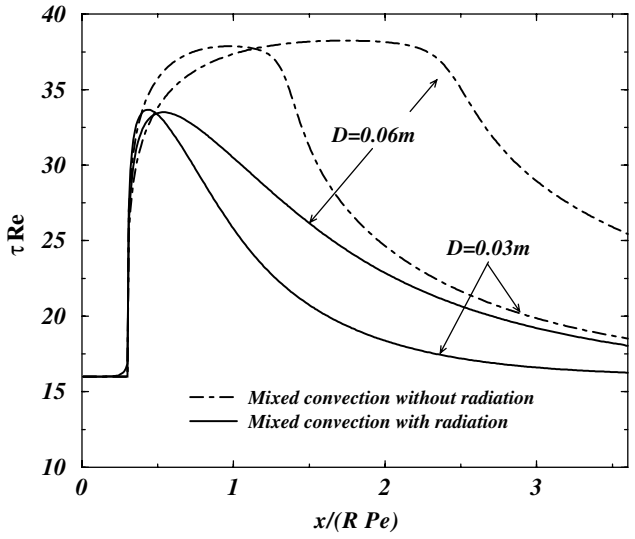

Fig. 3. Evolution of the local friction factor for heated pure H_2O flows; $T_0 = 400$ K, $T_w = 800$ K, $Re = 1000$ for $D = 0.03$ m, and $Re = 2390$ for $D = 0.06$ m.

account. Due to the axial propagation of radiation, the flow is slightly preheated and thus accelerated before the section $x = L_0$. However, the effect of this radiation preheating on the friction factor remains however very small (see Fig. 3).

In order to investigate the influence of gas radiative properties on thermal and velocity fields, the results obtained for H_2O, CO_2 and a H_2O–CO_2 mixture are compared. Fig. 4 illustrates the evolution of the non-dimensional axial centerline velocity $(u_c(x)/u_m(x))$ for $D = 0.03$ m, $T_0 = 400$ K, $T_w = 800$ K and $Gr/Re = 190$. It is seen that for mixed convection alone, the minimum value of (u_c/u_m) is the same for all gases. This result may be explained by the findings of Jeng et al. (1992) who

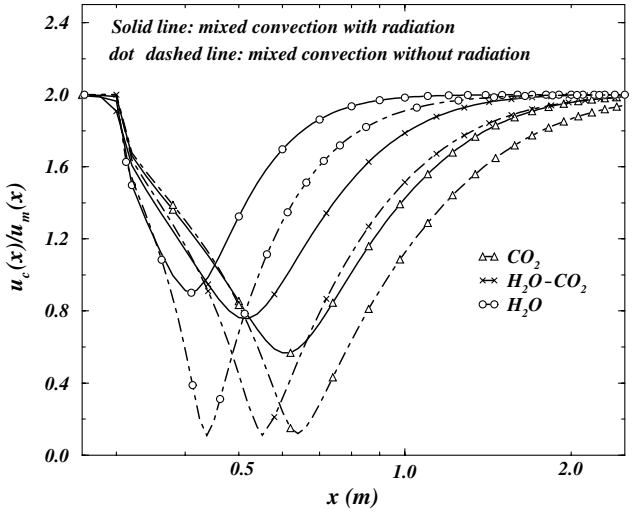

Fig. 4. Evolution of non-dimensional axial centerline velocity profiles for heated H_2O, CO_2 and H_2O–CO_2 mixture; $T_0 = 400$ K $T_w = 800$ K and $|Gr/Re| = 190$.

showed that, at sufficiently high Reynolds numbers and for fixed inlet flow and wall temperatures, and fixed Gr/Re ratio, some flow and thermal characteristics become independent of the Reynolds number. Fig. 4 shows that radiation increases the minimum value of u_c/u_m and that the magnitude of this effect depends on the flowing gas and, in particular, on its radiative properties. Water vapor is the most efficient species for bulk heating since its spectrum contains wide absorption bands. On the contrary, CO_2 has narrowest bands and the most intense one (near 4.3 μm) is so strong that radiative heating remains localized near the wall.

The evolution of axial velocity and temperature profiles, for a cooled H_2O case, are shown in Fig. 5. The bulk temperature evolves slowly towards the wall temperature compared to the heated case. In fact, although the total fluxes exchanged in both cases are of the same order (as will be shown later), the use of similar inlet Reynolds numbers leads to a higher mass flow rate in the cooling case due to the temperature-dependent viscosity, and then to a slower evolution of the bulk temperature. The effects of radiation on the velocity field is also less important than in the heating case. In addition to the slower temperature evolution, the relative variations of the density are smaller in the cooling case than in the heating one, which leads to only a small deceleration as observed in Fig. 5. It can also be noticed from this figure that this deceleration is more pronounced near the wall where radiative cooling of the fluid is a maximum and is added to the cooling by molecular diffusion.

Fig. 6 shows the axial evolution of the different fluxes exchanged per unit length for cooled and heated H_2O

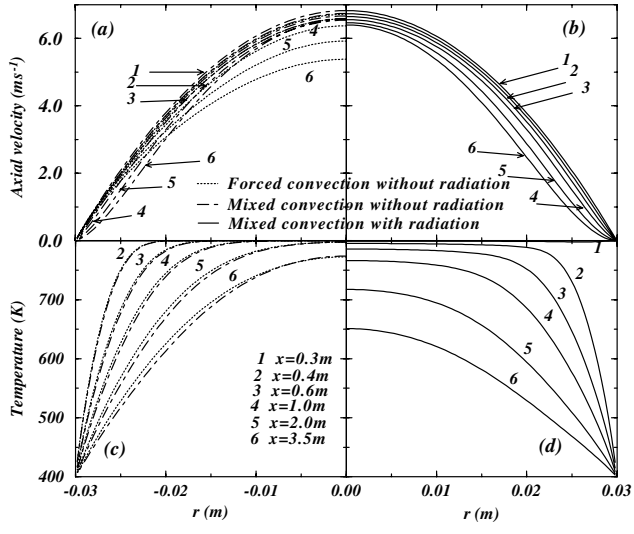

Fig. 5. Evolution of axial velocity and temperature profiles for cooled H_2O, $Re = 1900$ and $|Gr/Re| = 6.0$. Forced and mixed convection without radiation (a) and (c). Coupled mixed convection and radiation (b) and (d).

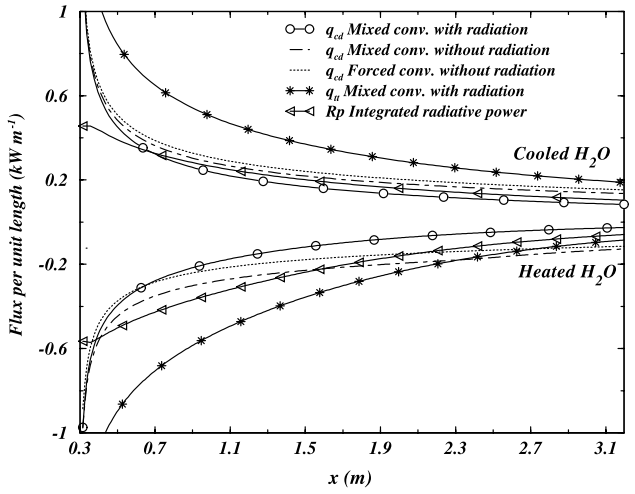

Fig. 6. Axial evolution of the different fluxes exchanged per unit length for heated H_2O flows ($T_0 = 400$ K, $T_w = 800$ K, $|Gr/Re| = 190$) and cooled H_2O flows ($T_0 = 800$ K, $T_w = 400$ K, $|Gr/Re| = 6.0$).

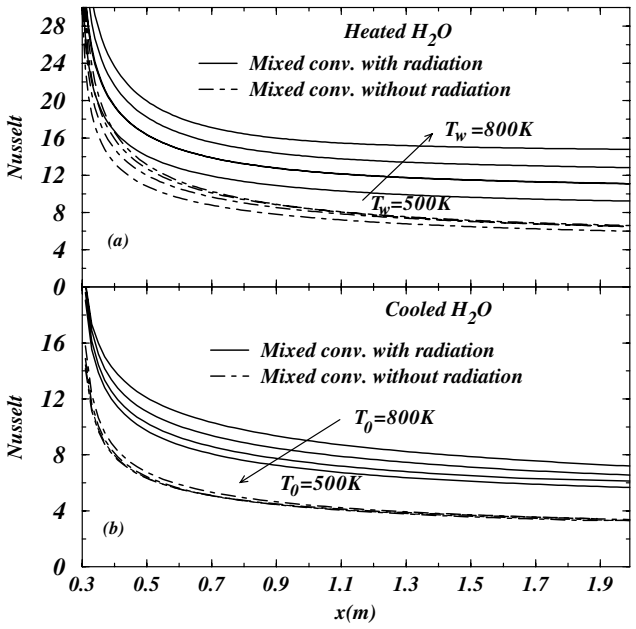

Fig. 7. Evolution of the total Nusselt number for (a) heated H_2O flows ($Re = 2390$; $T_0 = 400$ K; $T_w = 500$, 600, 700, and 800 K), and (b) cooled H_2O flows ($Re = 1900$; $T_w = 400$ K; $T_0 = 500$, 600, 700, and 800 K).

flows for $D = 0.06$ m. This figure shows the radiative fluxes exchanged by the gas per unit length (i.e., the radiative power per unit volume integrated over a cross section $R_P = \int_S \nabla \cdot \mathbf{q}_r \, dS$), the conductive flux $q_{cd}(x) = -2\pi R\lambda(T_w)(\partial T(x,r)/\partial r)|_{r=R}$ and the total flux $q_{tt}(x) = q_{cd}(x) + R_P(x)$. For comparison purposes, the conductive fluxes calculated without radiation, accounting or not for buoyancy effects are also plotted. Without radiation, the aiding buoyancy increases the conductive flux at the wall while this flux is decreased in the opposing buoyancy case. However, radiation enhances heat transfer for both cases and is more efficient than conductive transfer. Close to the thermal entrance, the orders of magnitude of the different fluxes are the same for heating and cooling cases. However, as the flow goes downstream, the fluxes decrease more quickly in the heated case since the bulk temperature evolves more rapidly towards the wall temperature. One can notice that radiative heat transfer decreases the conductive flux. This is mainly a result of smaller absolute differences between the bulk and wall temperature when radiation is taken into account.

Several calculations have been performed using different values of gas inlet and wall temperatures, as well as tube diameters and inlet Reynolds numbers in the domain allowed by the present model (laminar flow without reversal, see Section 3.2). The general trends and effects due to radiation, such as the enhancement of the total heat transfer, the increase in the centerline velocities for heated flows or, more generally, the reduction of gravity effects, are recovered when the physical parameters are changed.

Fig. 7 shows for instance the evolution of the total Nusselt numbers ($Nu = q_{tt}(x)/(|T_w - T_0|)$) obtained with and without radiation for different values of T_0 with $T_w = 400$ K for cooled flows, and of T_w with $T_0 = 400$ K for heated flows. In these calculations, the inlet Reynolds number is kept constant and the tube diameter is equal to 0.06 m. The Nusselt number computed without radiation is practically independent of T_w in the heated case, and on T_0 in the cooled case. When radiative transfer is taken into account, the total Nusselt number decreases as $|T_w - T_0|$ decreases since the global temperature level also decreases. Unfortunately, the results obtained with various physical parameters (T_w, T_0, Re, D, and gas mixture composition) cannot be put in general correlation formula since gas thermophysical properties depend strongly on the temperature, and radiative transfer depends in a highly non-linear manner on length scales and temperature levels. Although the results shown in Fig. 7 can be useful for engineering calculations as first order estimates, their use in other different conditions should be viewed with caution.

3.2. Radiation effects on the regime of reverse flow occurrence

As discussed previously, radiation has a strong effect on centerline velocities in the heating case and smaller effects near the wall in the cooling case. Therefore, it is expected that radiative transfer may significantly alter the regime of reverse flow occurrence. Although the boundary-layer model was adopted in this study, it is interesting to investigate qualitatively the effects of radiation on the possibility of flow reversal through the convergence or the divergence of our numerical procedure.

Previous works on mixed convection without radiation show that the marching procedure gives a good estimation of the location of the separation point and of the bulk temperature up to this point (Jeng et al., 1992). It was also shown that there is a close relation between flow reversal and numerical stability of the marching procedure because information is travelling in the direction opposite to the direction of marching when reverse flow occurs (Ingham et al., 1988; Jones and Ingham, 1994).

In order to check the ability of the marching procedure to predict the regime of reverse flow occurrence, we consider first a non-radiating fluid in the Boussinesq approximation and compare the results of available elliptic calculations with our marching procedure. Fig. 8a and b show comparisons between our results and those of Wang et al. (1994) and Zeldin and Schmidt (1972) for heating and cooling cases, respectively. The results are presented in the $(|Gr/Re|, Pe)$ plane. In our calculations, for fixed Prandtl and Grashof numbers, we started flow computations for a sufficiently high Reynolds number and decreased it gradually until the computations diverged. We checked that, just before the procedure divergence, the minimum value of axial velocity becomes negligibly small.

For the heating case, good agreement with the results obtained by Wang et al. (1994) is obtained for high values of Gr/Re. As Gr/Re decreases, the demarcation value tends to an asymptotic limit that is independent of Pe. Our parabolic calculations tend to $Gr/Re = 63$ while the calculations of Wang et al. (1994) tend to about 48 and Zeldin and Schmidt found $Gr/Re = 97$ for $Pe = 252.5$. The disagreement between the two elliptic calculations shows that the demarcation value of the separation point may be very sensitive to the numerical procedure.

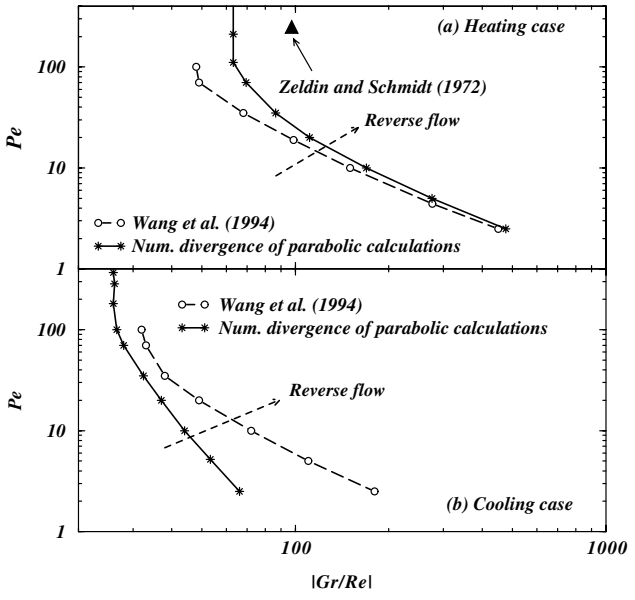

Fig. 8. Regimes of reverse flow occurrence for heating and cooling cases, mixed convection without radiation.

For the cooling case, flow reversal occurs near the wall and generally at smaller values of $|Gr/Re|$, approximately half of that for the heating case as pointed out by Wang et al. (1994). Only a qualitative agreement with the results of Wang et al. (1994) is obtained. However, here also, an asymptotic value of $|Gr/Re|$ has been found at high Pe values. The elliptic calculations predict $|Gr/Re| = 30$ for this asymptote while our calculations yield $|Gr/Re| = 26.1$. In summary, for non-radiating fluids and in the Boussinesq approximation, the marching procedure is shown to predict qualitatively the regimes of reverse flow occurrence but only fair quantitative agreement is obtained especially for cooling cases at small Pe values ($Pe < 50$).

In order to investigate radiation effects on reverse flow occurrence, we limit ourselves to $Pe > 100$ (i.e., in the asymptotic regime) and we consider H_2O as the flowing gas.

For real gases with non-gray and temperature-dependent spectra, flow conditions must be specified through primitive parameters such as tube diameter, wall and inlet temperatures, and not through non-dimensional numbers. The tube diameter is chosen between 0.03 and 0.1 m in such a way that, in the critical condition, the Peclet number is sufficiently high but the flows is still laminar. For fixed values of T_0, T_w and D (and thus inlet Grashof number), calculations are started for sufficiently high Reynolds number, which is then decreased until the divergence of the numerical procedure.

For heated water vapor, we impose $T_0 = 400$ K while T_w varies from 400 to 1000 K. Fig. 9 shows the stability limits for three tube diameters, with and without radiation, in terms of $|Gr/Re|$ vs $|T_w - T_0|/T_0$. The stability limit for H_2O, assumed to be transparent, is found to be independent of the diameter since the flows are in the asymptotic limit at high Peclet numbers. It is shown on Fig. 9 that radiative transfer increases the critical Gr/Re value by a factor up to 50. As discussed previously, this is the result of radiative bulk heating of the flow and the resulting important increase of centerline axial velocity. The delay of reverse flow occurrence is more and more important as the optical thickness of the medium increases.

For cooled water vapor, we impose $T_w = 400$ K while T_0 is varied from 400 to 1000 K. Fig. 10 shows the critical $|Gr/Re|$ values vs $|T_0 - T_w|/T_0$. Calculations without radiation show that the critical value decreases as T_0 increases. This is simply the result of viscosity variations with T_0 and of the fact that $|Gr/Re|$ scales as $(T_0 - T_w)/(\mu T_0^2)$ which decreases strongly when T_0 increases. The effects of radiation on the stability limits as shown to be very small for cooled gases. In fact, flow

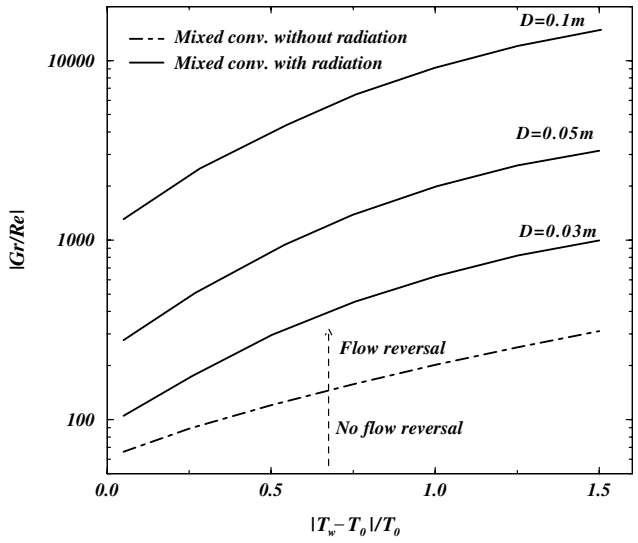

Fig. 9. Effect of thermal radiation on the regime of reverse flow occurrence for heated pure H_2O.

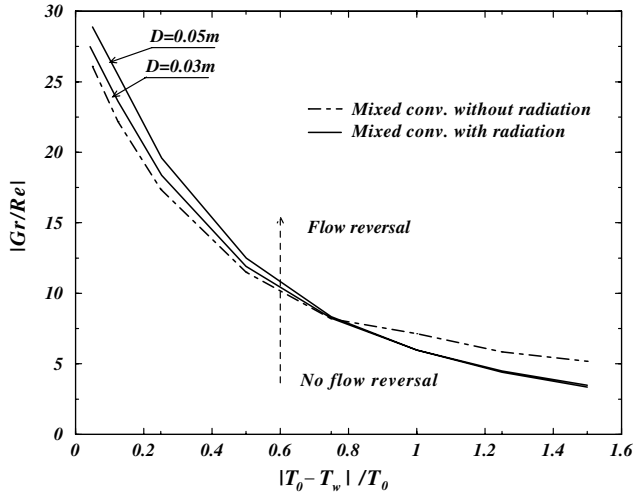

Fig. 10. Effect of thermal radiation on the regime of reverse flow occurrence for cooled pure H_2O.

reversal occurs in a region adjacent to the wall and of very small optical thickness. Radiative transfer may slightly increase or decrease the critical $|Gr/Re|$ value depending on the sign of the radiative power in the region where the flow is being reversed.

4. Conclusion

The interaction between thermal radiation and mixed convection in laminar ascending gas flows in vertical tubes has been studied. Attention was paid to real gas effects: radiative properties of H_2O, CO_2 and H_2O–CO_2 mixtures have been taken into account through the ADF model, and temperature-dependent thermophysical properties were considered. In both cases, radiation enhances heat transfer and speeds up the evolution of bulk temperature towards wall temperature. In the heating case, the propagation of radiation towards the central region of the duct tends to increase the centerline velocity and decreases the friction factor. This induces a significant increase of the critical Gr/Re ratio corresponding to reverse flow occurrence. For the cooling case, reverse flow occurs in a region adjacent to the hot wall. As this region is optically thin, radiation has a small effect on the regime of reverse flow occurrence. A natural extension of this investigation will be the development of a fully coupled elliptic model which will be able to predict more precisely the critical limits of the reverse flow occurrence in presence of radiation, and to study radiation effects on recirculating flows.

References

Aung, W., Worku, G., 1986a. Developing flow and flow reversal in a vertical channel with asymmetric wall temperatures. J. Heat Transfer 108, 299–304.

Aung, W., Worku, G., 1986b. Theory of fully developed combined convection including flow reversal. J. Heat Transfer 108, 485–488.

Aung, W., Moghadam, H.E., Tsou, F.K., 1991. Simultaneous hydrodynamic and thermal development in mixed convection in a vertical annulus with fluid property variation. J. Heat Transfer 113, 926–931.

Backstron, C.A., McEligot, D.M., 1970. Turbulent and laminar heat transfer to gases with varying properties in the entry region of circular ducts. Int. J. Heat Mass Transfer 13, 319–343.

El-Shaarawi, M.A.I., Sarhan, A., 1981. Developing laminar free convection in a heated vertical open-ended concentric annulus. Ind. Eng. Chem. Fundam. 20, 388–394.

Gau, C., Yih, K.A., Aung, W., 1992a. Reversed flow structure and heat transfer measurements for buoyancy-assisted convection in a heated vertical duct. J. Heat Transfer 114, 928–935.

Gau, C., Yih, K.A., Aung, W., 1992b. Measurements of heat transfer and flow structure in heated vertical channels. J. Thermophys. Heat Transfer 6, 707–712.

Habchi, S., Achaya, S., 1986. Laminar mixed convection in a symmetrically or asymmetrically heated vertical channel. Numer. Heat Transfer 9, 605–618.

Heggs, P.J., Ingham, D.B., Keen, D.J., 1990. The effects of heat conduction in the wall on the development of recirculating combined convection flows in vertical ducts. Int. J. Heat Mass Transfer 33, 507–528.

Ingham, D.B., Keen, D.J., Heggs, P.J., 1988. Flow in vertical channel with symmetric wall temperatures and including situations where reverse flows occur. J. Heat Transfer 110, 910–917.

Ingham, D.B., Keen, D.J., Heggs, P.J., Morton, B.R., 1990. Recirculating pipe flow. J. Fluid Mech. 213, 443–464.

Jackson, J.D., Cotton, M.A., Axcell, B.P., 1989. Studies of mixed convection in vertical tubes. Int. J. Heat Fluid Flow 10, 2–15.

Jeng, Y.N., Chen, J.L., Aung, W., 1992. On the Reynolds-number independence of mixed convection in a vertical channel subjected to asymmetric wall temperatures with and without flow reversal. Int. J. Heat Fluid Flow 13, 329–339.

Jones, A.T., Ingham, D.B., 1994. Combined convection flow and heat transfer to a power law fluid in a vertical duct, including reverse situations. Numer. Heat Transfer, Part A 25, 57–73.

Marner, W.J., McMillan, H.K., 1970. Combined free and forced convection laminar heat transfer in a vertical tube with constant wall temperature. J. Heat Transfer 92, 559–562.

Morton, B.R., Ingham, D.B., Keen, D.J., Heggs, P.J., 1989. Recirculating combined convection in laminar pipe flow. J. Heat Transfer 111, 106–113.

Nesreddine, H., Galanis, N., Nguyen, C.T., 1998. Effects of axial diffusion on laminar heat transfer with low Peclet numbers in the entrance region of thin vertical tubes. Numer. Heat Transfer, Part A 33, 247–266.

Pierrot, L., Rivière, Ph., Soufiani, A., Taine, J., 1999a. A fictitious-gas-based absorption distribution function global model for radiative transfer in hot gases. J. Quant. Spectrosc. Radiat. Transfer 62, 609–624.

Pierrot, L., Soufiani, A., Taine, J., 1999b. Accuracy of narrow-band and global models for radiative transfer in H_2O, CO_2, and H_2O–CO_2 mixtures at high temperature. J. Quant. Spectrosc. Radiat. Transfer 62, 523–548.

Rivière, Ph., Langlois, S., Soufiani, A., Taine, J., 1995. An approximate data base of H_2O infrared lines for high temperature applications at low resolution. Statistical narrow-band models parameters. J. Quant. Spectrosc. Radiat. Transfer 53, 221–234.

Scutaru, D., Rosenman, L., Taine, J., 1994. Approximate band intensities of CO_2 hot bands at 2.7, 4.3 and 12 μm for high and medium resolution applications. J. Quant. Spectrosc. Radiat. Transfer 52, 765–781.

Sediki, E., Soufiani, A., Sifaoui, M.S., 2002. Spectrally correlated radiation and laminar forced convection in the entrance region of a circular duct. Int. J. Heat Mass Transfer 45, 5069–5081.

Taine, J., Soufiani, A., 1999. Gas IR radiative properties: from spectroscopic data to approximate models. In: Advances in Heat Transfer, vol. 33. Academic Press, New York, pp. 295–414.

Touloukian, Y.S., Liley, P.E., Saxena, S.C., 1970a. In: Thermophysical Properties of Matter, vol. 3. IFI/Plenum, New York/Washington.

Touloukian, Y.S., Saxena, S.C., Hestermans, P., 1970b. In: Thermophysical Properties of Matter, vol. 11. IFI/Plenum, New York/Washington.

Viskanta, R., 1998. Overview of convection and radiation in high temperature gas flows. Int. J. Eng. Sci. 36, 1677–1699.

Wang, M., Tsuji, T., Nagano, Y., 1994. Mixed convection with flow reversal in the thermal entrance region of horizontala and vertical pipes. Int. J. Heat Mass Transfer 37, 2305–3219.

Worsoe-Schmidt, P.M., Leppert, G., 1965. Heat transfer and local friction for laminar flow of gas in a circular tube at high heating rate. Int. J. Heat Mass Transfer 8, 1281–1301.

Yan, W.M., Li, H.Y., 1997. Radiation effects on laminar mixed convection in an inclined square duct. In: Proceedings of the ASME Heat Transfer Division, HTD, vol. 353, pp. 233–242.

Yan, W.M., Li, H.Y., 2001. Radiation effects on mixed convection heat transfer in a vertical square duct. Int. J. Heat Mass Transfer 44, 1401–1410.

Yang, L.K., 1991. Combined mixed convection and radiation in a vertical pipe. Int. Commun. Heat Mass Transfer 18, 419–430.

Yang, L.K., 1992. Forced convection in a vertical pipe with combined buoyancy and radiation effect. Int. Commun. Heat Mass Transfer 19, 249–262.

Zeldin, B., Schmidt, F.W., 1972. Developing flow with combined forced-free convection in an isothermal vertical tube. ASME, J. Heat Transfer 94, 211–223.

Zhang, L., Soufiani, A., Taine, J., 1988. Spectral correlated and non-correlated radiative transfer in a finite axisymmetric system containing an absorbing and emitting real gas-particle mixture. Int. J. Heat Mass Transfer 31, 2261–2272.